ELSEVIER

Journal of Alloys and Compounds 293–295 (1999) 663–669

Journal of ALLOYS AND COMPOUNDS

About the mechanism and the rate limiting step of the metalhydride electrode reaction

A. Züttel[a,*], V. Güther[b], A. Otto[b], M. Bärtsch[c], R. Kötz[c], D. Chartouni[a], Ch. Nützenadel[a], L. Schlapbach[a]

[a]*University of Fribourg, Physics Institute, Pérolles, CH-1700 Fribourg, Switzerland*
[b]*Gesellschaft für Elektrometallurgie (GfE), Höfener Strasse 45, D-90431 Nürnberg, Germany*
[c]*Paul Scherrer Institute (PSI), CH-5232 Villigen, Switzerland*

Abstract

$LaNi_5$ alloy powder samples absorb in the gas phase 80% of their maximum hydrogen capacity (H/M=6) in less than 30 seconds. In the electrochemical discharge process, the charge transfer at the surface of the negative electrode should be the rate determining step because an electrochemical discharge reaction is about an order of magnitude slower than a gas phase desorption process. In this study the alloy system $Lm(Ni_{3.6}Co_{0.7}Al_{0.3}Mn_{0.4})_\alpha$ with $0.96 \leq \alpha \leq 1.12$ was examined as a model system. The reaction resistance of the electrodes was directly measured by means of impedance spectroscopy as a function of the hydrogen concentration in the metalhydride. The high rate dischargeability as well as the resistance are related to the surface composition and surface morphology. The surface composition of a metalhydride electrode not only varies with the cycle number but also changes within a single cycle.

Keywords: Metalhydride; AB_5; Kinetics; Electrochemistry; Reaction resistance

1. Introduction

The literature concerning kinetics of MH-electrodes is mainly based on the improvement of the rate of activation of the electrodes. Sawa et al. [1] investigated an oxidation treatment which improved the activity of the electrodes and increased the corrosion resistance during cycling of some Ti–Zr–V-alloy electrodes. Oxidation treatment was carried out by annealing the electrode under low pressure oxygen (15–75 mbar) at a temperature of 250–300°C. This oxidation treatment was found to be effective especially for zirconium rich alloys. Iwakura et al. [2] modified the surface of $MmNi_{3.6}Mn_{0.4}Al_{0.3}Co_{0.7}$ alloy electrodes by the reducing agent H_3PO_2 and observed an increased high-rate dischargeability and higher discharge capacity. This effect is explained by reduction and elimination of oxides on the surface of the alloy particles. Matsuoka et al. [3] used 6 M KOH solution containing 0.001–0.1 M KBH_4 as reducing agent at 80°C to modify the surface of $MmNi_{3.6}Mn_{0.4}Al_{0.3}Co_{0.7}$ alloy electrodes. The electrocatalytic activity of the electrodes increased by eliminating barrier films from the surface of the alloys. Furthermore, during the surface modification hydride formation was observed. The uptake of hydrogen being released from KBH_4 is also effective in increasing catalytic activity because of the decrepitation of the alloy particles.

Kuriyama [4] characterized metal hydride electrodes by means of electrochemical impedance spectroscopy. Resistive components of various metal hydride electrodes were evaluated. Examples of applications of the technique are the characterization of the difference in performance between a mischmetal-based alloy ($MmNi_{3.5}Co_{0.7}Al_{0.8}$) electrode and a titanium-based alloy electrode. Kuriyama [5] also investigated the deterioration behavior of metal hydride electrodes by means of electrochemical impedance spectroscopy. Cole–Cole plots for the electrodes consist of two obvious semicircles and a slope related to the Warburg impedance. The semicircle in the high-frequency region was mainly related to the resistance and capacitance between the current collector and the pellet of alloy powder. The semicircle in the low-frequency region, which exhibited appreciable dependence on hydrogen content, was attributed to the electrode reactions on the alloy particles and double-layer capacitance on the alloy par-

*Corresponding author. Tel.: +41-26-300-9086; fax: +41-26-300-9747.

E-mail address: Andreas.Zuettel@unifr.ch (A. Züttel)

0925-8388/99/$ – see front matter
PII: S0925-8388(99)00427-2

ticles. Resistance and capacitance between alloy particles in the electrodes also need to be taken into account. According to Kuriyama the resistances of a metal hydride electrode can be divided into a part given by the morphology and a part given by the reaction barrier. Approximately only one third of the total resistance in the measurement is due to the reaction resistance. Two thirds were due to the electrode's morphology dependent resistance. The reaction resistance and the resistance of the electrolyte are strongly temperature dependent. A decrease of 10°C in temperature doubles the reaction resistance and the conductivity of the electrolyte decreases by approximately 30%.

Züttel et al. [6] investigated the influence of the electrode thickness on the overpotential during charge and discharge using a $MmNi_{3.6}Mn_{0.3}Al_{0.4}Co_{0.7}$ (Lm: 52% La, 33% Ce, 11% Nd, 3% Pr) alloy. The unsigned value of the overpotentials are equal for charge and discharge. The charge/discharge kinetics are expected to depend on the reaction mechanism and on the electrode morphology. The analysis of a series of electrodes with different thickness has demonstrated that the resistance increases linearly with the thickness of the electrode: R [Ωg]=0.06 Ωg+0.42 Ωgmm^{-1}d [mm]. The porosity of the electrodes was found to be 24%.

Fukumoto [7] investigated the effect of the stoichiometric ratio on the electrochemical properties of negative electrodes for the alloys $Mm(Ni_{3.6}Mn_{0.4}Al_{0.3}Co_{0.7})_\alpha$(Mm: 52.6% Ce, 24.9% La, 5.6% Pr, 16.9% Nd and 0.14% Sm) and $0.88 \leq \alpha \leq 1.12$. The unit cell volume as well as the discharge capacity (i_{dis}=200 mAg^{-1}) of the alloys decreases in the range of $0.96 \leq \alpha \leq 1.12$. In the same range of α the plateau pressure increases, i.e. the stability of the hydrides decreases. The exchange current density depends linearly on the plateau pressure: i [mAg^{-1}]=415+100 p [bar].

Iwakura et al. [8] determined the activation energy for hydrogen absorption of the electrodes from the peak current in the polarisation curve. The activation energy (E_a) for the hydrogen absorption reaction of a series of $Mm(Ni_{3.6}Mn_{0.4}Al_{0.3}Co_{0.7})_\alpha$ with $0.88 \leq \alpha \leq 1.12$ alloys depends on α according to the following equation: E_a [kJmol^{-1}]=10.4+72.6α−56.3α^2. Furthermore, it was shown that the discharge efficiency correlates linearly with the activation energy as well as with the exchange current density.

During the discharge process, either hydrogen diffusion in the bulk of the alloy or the charge transfer at the surface of the metal hydride electrode should be the rate determining step [9]. Since the alloy with the composition α=0.88 forms a more stable hydride, it is supposed that the rate of hydrogen diffusion is relatively slow, resulting in a smaller discharge capacity.

Percheron-Guégan et al. [10] investigated the hydrogen absorption rate of $LaNi_5$ alloy powder in the gas phase. The samples absorbed 80% of their maximum capacity (H/M=6) in less than 30 seconds. Comparing this result with the electrochemical measurements leads to the conclusion that bulk diffusion as well as nucleation and growth of the β-phase can not be rate determining in the electrochemical charge reaction, because this part of the reaction is identical for electrochemical and gas phase absorption.

In this paper the alloy system $Lm(Ni_{3.6}Co_{0.7}Al_{0.3}Mn_{0.4})_\alpha$, Lm: lanthanum rich mischmetal ≈50 wt.% La, with $0.96 \leq \alpha \leq 1.10$ was investigated. The desorption rates of the electrochemical reaction are investigated and the reaction resistances are analyzed in detail.

2. Experimental

2.1. Alloy preparation

Three alloys with the composition $Lm(Ni_{3.6}Mn_{0.4}Al_{0.3}Co_{0.7})_\alpha$ (Lm: 50% La, 35% Ce, 3.5% Pr, and 11% Nd) and α=0.96, 1.02 and 1.12 ($AB_{4.82}$, $AB_{5.08}$ and $AB_{5.48}$) were melted in a vacuum induction furnace. The alloys were annealed for 4 hours at 900°C.

2.2. Structural analysis

The alloys were first broken with a hammer and then powdered using a mortar. X-ray diffraction was performed with copper radiation (Cu K_α radiation: λ_1=1.540600 Å, λ_2=1.544380 Å, I_2/I_1=50%, T=298 K).

2.3. Electrochemical tests

For the electrochemical measurements approximately 25 mg of the alloy powder was mixed with copper powder (Merck p.a. <63 μm) in the weight ratio of 1:3 and cold pressed (p=500 MPa) to a pellet (d=7 mm). The pellets were fixed on a nickel holder with a cylindrical PTFE-clip. The electrodes were charged and discharged electrochemically in a 6 M KOH electrolyte in an open standard electrochemical cell. A nickel plate was used as counter electrode and potentials were referred to a Hg/HgO reference electrode [12]. The discharge cut-off potential was set to −0.6 V vs. Hg/HgO reference electrode. The electrodes were cycled with constant charge and discharge current (300 mAg^{-1}).

2.4. Equilibrium potential measurements

The equilibrium potentials were measured with pulsed cycle method, i.e. the current was applied for a short time (8 minutes) and after a pause of 3 minutes the potential was measured. This procedure was repeated 50 times until the electrode was completely charged. After that the equilibrium potential of the discharge branch was determined with the same method.

2.5. Deep discharge

Upon 30 activation cycles the electrodes were completely discharged, i.e. deeply discharged. The electrodes were first discharged with the nominal discharge current of 5000 mAg^{-1} until the cutoff potential of −0.6 V was reached. After a rest time of 3 minutes (open circuit) a discharge at a smaller current (3100 mAg^{-1}) was carried out. This procedure was repeated several times and the capacity for each discharge current was calculated from the discharge time separately. The sum of all the capacities is referred to as the maximum capacity.

2.6. Impedance spectroscopy

The electrode resistance as a function of the equilibrium potential was determined by impedance spectroscopy. The electrodes were first equilibrated for one hour at a certain potential before the impedance measurement was started at 100 kHz. The bias was set to the equilibrium potential and a sinusoidal potential was applied with an amplitude of 10 mV.

2.7. Potential step

In order to compare constant pressure gas phase absorption measurements and electrochemical measurements the electrodes were set to a constant potential and the current was measured. The current represents the rate of absorption or desorption and the integrated current corresponds to the change capacity.

2.8. X-ray photoelectron spectroscopy (XPS) measurements

Copper free pellets were prepared for XPS-analysis by pressing only the alloy powder to a pellet. For the surface analysis samples were rinsed with bidistilled water, dried in air and subsequently introduced in the ultra high vacuum ($<10^{-8}$ Pa base pressure, 10^{-7} Pa H_2 partial pressure after introducing the degassing samples) chamber of the spectrometer. The surface concentration of the elements was analyzed with XPS in a VG ESCALAB 5 spectrometer using MgK_α radiation of 1253.6 eV (Au $4f_{7/2}$ at 84.0 eV, 1.7 eV FWHM). The measured surface composition is an average over an area of 0.2 cm^2 and a depth of 10–30 Å. The sputter depth profiles (Ar^+, 2 keV) were evaluated using a standard rate of 500 Å cm^2 min^{-1} mA^{-1} (4 Å/min.) and are therefore only to a factor of 2 precise in depth, due to the element specific sputtering rate and the analyzing depth. The most significant differences in the depth profiles are observed within the top 50–100 Å. As the probing depth of XPS is ~30 Å and the depth resolution upon sputtering is 20–30 Å, the top layer can not be probed in more detail.

3. Results and discussion

3.1. Crystal structure

The $AB_{5\pm\varepsilon}$ alloys crystallize in a hexagonal structure (Struc. type: $CaCu_5$, Pearson symb.: hP6, s.g. *P6/mmm*, #191). Lanthanum and cerium occupies the 1*a* site (0, 0, 0), the aluminum atoms occupies only the 3*g* sites (1/2, 0, 1/2), manganese is preferentially (82%) found on 3*g* sites and a small amount (18%) on 2*c* sites (1/3, 2/3, 0). The cobalt atoms occupy both sites (25%) 2*c* and (75%) 3*g* [11]. The X-ray diffraction patterns are shown in Fig. 1 and the lattice parameters and the unit cell volume are listed in Table 1. The FWHM (full width at half maximum) of the diffraction peaks decreases with increasing α. This indicates that the alloys crystallize more properly if the ratio of A to B elements decreases. The unit cell volume decreases with increasing stoichiometry. This behavior is in good agreement with the results obtained by Fukumoto [7]. However, the unit cell volume of the alloys in this study is approximately 0.7% larger compared to the unit cell volume given in Fukumoto's publication. The reason for the difference may originate in the different mischmetal composition. Fukumoto used a mischmetal containing about 53% cerium while the mischmetal used in this study contains about 50% lanthanum and 35% cerium.

3.2. Equilibrium hydrogen pressure

The electrochemical equilibrium potential and the hydrogen equilibrium pressure are related with the Gibb's free energy (see Appendix A) The pressure–concentration isotherms of the investigated alloys exhibit no well defined plateau. In order to determine an absorption and desorption potential the density of states (DoS) for hydrogen in the host metal were calculated. The density of states is simply the derivative of the capacity (C) by the equilibrium potential (E_{eq}).

$$\mathrm{DoS} = \frac{\mathrm{d}C}{\mathrm{d}E_{eq}}$$

The DoS as a function of the equilibrium potentials and equilibrium pressures are presented in Fig. 2. The equilibrium plateau pressure can be determined as the center of the distribution. The distribution moves to higher pressures with increasing α. Furthermore, the distribution of the DoS becomes more narrow with increasing stoichiometry, i.e. increasing α. This is in good agreement with the decreasing unit cell volume and the decreasing ratio of A/B elements with increasing α. The unit cell volume as well as the ratio of the A/B elements influences the hydrogen equilibrium plateau pressure. A smaller unit cell volume leads to an increase in equilibrium pressure. Furthermore the lower chemical affinity of B elements to hydrogen also

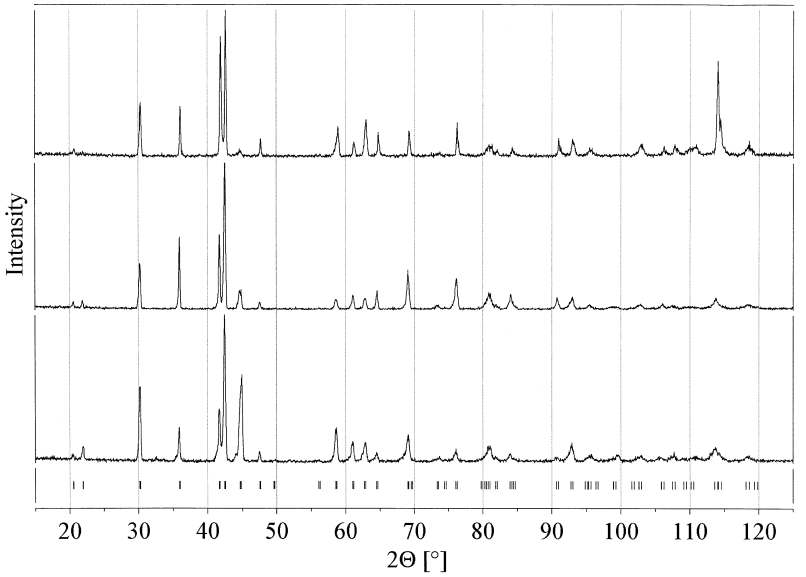

Fig. 1. X-Ray diffraction pattern for the $Lm(Ni_{3.6}Co_{0.7}Al_{0.3}Mn_{0.4})_{\alpha}$ alloy samples. $\alpha=0.96$ on bottom, $\alpha=1.02$ middle and $\alpha=1.12$ on top. Cu K_{α} radiation: $\lambda_1=1.54060$ Å, $\lambda_2=1.54438$ Å, $T=298$ K.

leads to an increase of the equilibrium pressure for increasing α.

3.3. Discharge capacity

The discharge capacities were measured as a function of the discharge current. This type of measurement is dynamic (nonequilibrium), it involves all the electrode processes, e.g. charge transfer, diffusion of hydrogen in the host metal, phase transition etc. The maximum capacity as a function of the discharge time (measured discharge capacity divided by the discharge current) was calculated and is shown in Fig. 3. The discharge capacity is almost independent of the discharge time as long as the discharge time is greater than one hour. The stoichiometric alloy ($\alpha=1.02$) shows the highest discharge capacity over the whole range of the investigated discharge currents.

3.4. Reaction resistance

The reaction resistance of the metal hydride electrode was determined by means of impedance spectroscopy. Fig. 4 shows a typical impedance spectrum for the type of electrodes used in this study. The impedance spectrum in Fig. 4 was measured just below the hydrogen evolution at −16 mV. Five different resistances (R_1, R_2, R_3, R_4, W,

Table 1
Lattice parameter (a, c) of the hexagonal $CaCu_5$ structure, the unit cell volume and the molecular weight for the three different stoichiometries including the hydrides

	a [Å]	c [Å]	V [Å^3]	M [g mol^{-1}]
$A(B_5)_{0.96}$	5.012	4.0508	88.11	410.9
$A(B_5)_{0.96}H_x$	5.296	4.191	101.8	
$A(B_5)_{1.02}$	5.0057	4.0508	88.01	427.9
$A(B_5)_{1.02}H_x$	5.268	4.178	100.4	
$A(B_5)_{1.12}$	4.996	4.0606	87.77	450.5

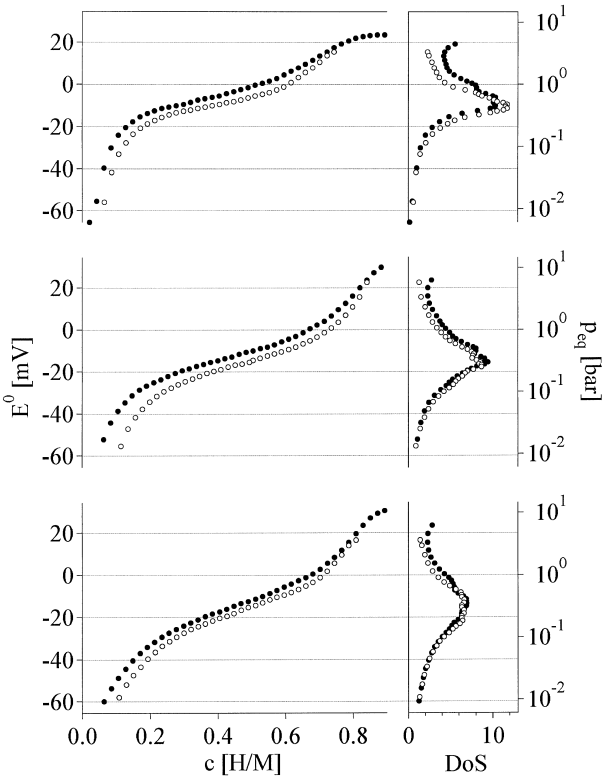

Fig. 2. Equilibrium potential versus hydrogen concentration and density of states for hydrogen in the host metal determined from electrochemically measured potential–capacitance isotherms for the $Lm(Ni_{3.6}Co_{0.7}Al_{0.3}Mn_{0.4})_{\alpha}$ alloy samples. $\alpha=0.96$ on bottom, $\alpha=1.02$ middle and $\alpha=1.12$ on top ($T=298$ K). Absorption measurement (●) and desorption measurement (○).

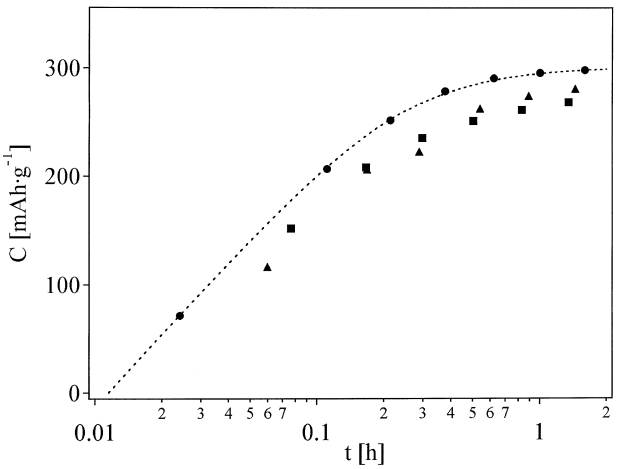

Fig. 3. Maximum discharge capacity which can be achieved in a certain discharge time for the $Lm(Ni_{3.6}Co_{0.7}Al_{0.3}Mn_{0.4})_{\alpha}$ alloy samples, (▲) $\alpha=0.96$, (●) $\alpha=1.02$ and (■) $\alpha=1.12$ ($T=298$ K). The time (t) is the ratio of the discharge capacity divided by the discharge current $t=C_{max}/i_{dis}$.

measured as the diameter of the semicircles) can be distinguished. The resistance at very high frequencies (R_1, $f>100$ kHz) is 0.03 Ωg and independent of the electrode potential. This resistance is attributed to the electrolyte and depends on the distance between the reference and the work electrode, the type of electrolyte and the concentration of the electrolyte. The second resistance R_2 is found at a frequency of 4 kHz. This resistance is quite small at −16 mV, only 0.007 Ωg, and increases for more positive potentials. R_2 is attributed to the contact between the metal hydride bed and the current collector. This contact resistance depends on the chemical state of the contact surface and on the thickness of the oxide layers. The growth of an oxide layer is a function of the electrochemical potential of the electrode. Therefore this resistance depends on the potential of the electrode. The third resistance R_3 is attributed to the grain to grain contact in the metal hydride bed and is 0.006 Ωg. This resistance is mainly affected by the compacting method and the pressure applied to the electrode. Due to the large amount of copper (75%) used in the electrodes, the grain to grain contact resistance varies only little as a function of the potential. The fourth resistance R_4 at a frequency of 2 Hz is attributed to the reaction resistance and is 0.07 Ωg at a potential of −16 mV. This is the most important part of the overall electrode resistance. The reaction resistance is defined by the interaction of water molecules with the alloy surface and depends therefore on the alloy and especially the surface composition of the alloy. Finally below a frequency of 50 mHz we find the Warburg impedance *W*.

The reaction resistance strongly depends on the electrode potential as shown in Fig. 5. This resistance is almost independent of the electrode potential for negative potentials, because of the high concentration of hydrogen atoms at the surface of the alloy. The hydrogen atoms at the surface prevent the metals from being further oxidized. The reaction resistance increases only little in the potential range where the phase transition occurs. Within the small potential region of the phase transition the metal hydride absorbs and desorbs a large amount of hydrogen. The reaction resistance increases over two orders of magnitude in the solid solution phase (α-phase). The main reason for this behavior is the oxidation of nickel and cobalt around a potential of 0.1 V vs. the hydrogen electrode. At more positive potentials some species at the alloy surface

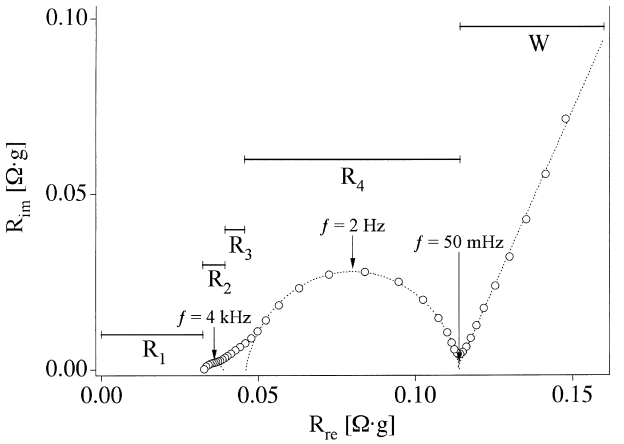

Fig. 4. Impedance spectrum of the the alloy $Lm(Ni_{3.6}Co_{0.7}Al_{0.3}Mn_{0.4})_{1.02}$ ($AB_{5.08}$) electrode measured in the completely charged state just below the hydrogen evolution at $E^0=-0.016$ V ($T=298$ K). The first measured point is at $R_{re}=0.04$ Ωg ($f=100$ kHz). The spectrum shows a high frequency semicircle with the center at $R_{re}=0.036$ Ωg ($f=4$ kHz) and a diameter of 0.007 Ωg followed by a second semicircle with a center at $R_{re}=0.08$ Ωg ($f=2$ Hz) and a diameter of 0.07 Ωg. Below $f=50$ mHz a linear relationship is observed: $R_{im}=-11.472+2.0251R_{re}$, the so called Warburg impedance.

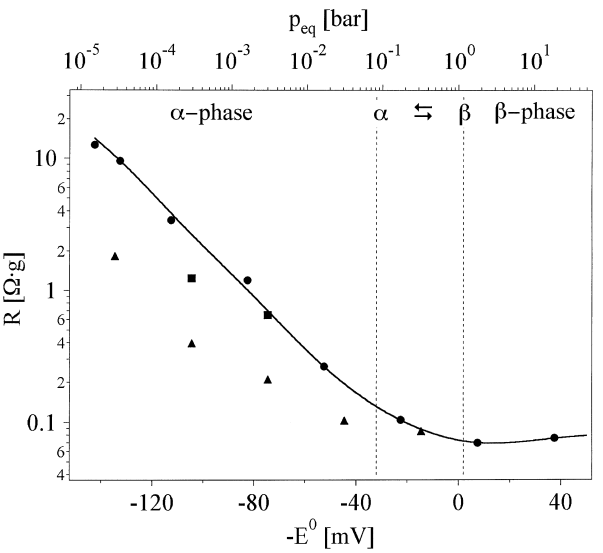

Fig. 5. Reaction resistance as a function of the electrode potential for the $Lm(Ni_{3.6}Co_{0.7}Al_{0.3}Mn_{0.4})_{\alpha}$ alloy samples, (▲) $\alpha=0.96$, (●) $\alpha=1.02$ and (■) $\alpha=1.12$ ($T=298$ K). The resistance was determined from the diameter of the low frequency semicircle.

oxidize and therefore the electrical resistance increases drastically.

When a current is applied to the electrode the resistance of the electrode is responsible for the overpotential i.e. the difference between the electrode potential and the equilibrium potential. During the charge reaction the overpotential pushes the electrode potential to a more negative value into the potential range where the resistance is low and almost independent of the potential. However, during the discharge reaction the opposite effect is observed and the electrode potential is pushed to a more positive value into the range where the resistance increases as a function of the potential. Furthermore, the increase of the reaction resistance leads to an even higher overpotential and therefore to a higher resistance. This amplification effect on the electrode resistance is responsible for the very low capacities which a metal hydride electrode delivers at high discharge currents.

3.5. Surface composition

The surface composition of the $AB_{4.82}$ alloy was determined by XPS depth profiling (Fig. 6). The analysis on the sample is difficult due to the large number of elements in the alloy. We have analyzed an untreated metallic powder sample and the same alloy powder upon 11 electrochemical activation cycles. The untreated powder sample represents the electrode with a high resistance and the activated sample represents the electrode with a low resistance. The untreated powder shows an enrichment of A-elements at the top surface. These elements are completely oxidized. The oxygen concentration decreases within the first 50 Å to a constant level close to zero. This compact metal oxide layer at the surface of the alloy particles together with the low concentration of nickel at the top surface is a barrier for the hydrogen penetration as well as for the electron transfer.

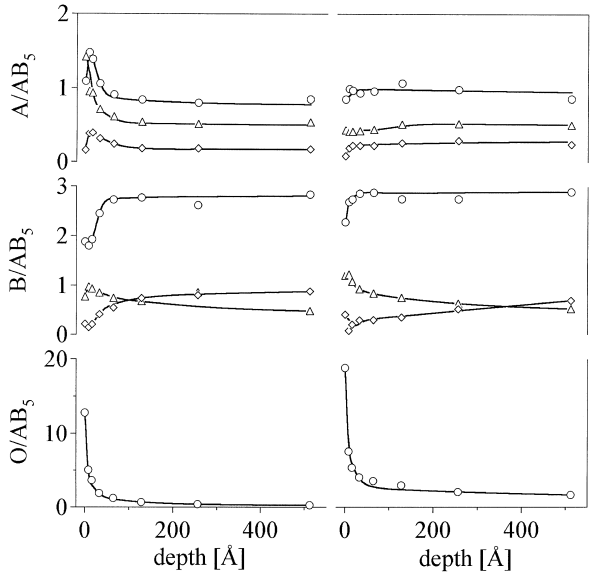

Fig. 6. Elemental composition as a function of depth for the $AB_{5.08}$ alloy as received (left hand side) and upon 10 electrochemical cycles (right hand side). The relative amount of A-elements (La: ○, Ce: △, Nd: ◇) on top, B-elements (Ni: ○, Co: ◇, Mn: △) in the middle and oxygen on bottom.

The activated sample (11 cycles) shows a very different concentration profile. A part of the oxidized A-elements is dissolved in the electrolyte, and the concentration of the A-elements is almost constant over the whole analyzed depth (500 Å). The concentration of nickel at the surface is strongly increased compared to the concentration of the untreated alloy. Nickel acts as electron conductor, as a catalyst for water dissociation and provides sites for the chemisorption of hydrogen.

4. Conclusion

The unit cell of the investigated alloys increases as well as the equilibrium plateau potential increases, and the DoS distribution becomes more narrow with increasing stoichiometry (α). The high rate dischargeability is best for the stoichiometric compound ($\alpha = 1.02$) because this alloy also exhibited the highest discharge capacity. However, the dependence of the capacity on the current is very similar for all the investigated alloys.

The lowest reaction resistance was found for the understoichiometric alloy ($\alpha = 0.96$). Upon activation of the alloy electrode, the surface composition changes. A part of the oxidized A-elements dissolve in the electrolyte and nickel concentration increases in the top surface layer.

The surface composition of the alloy determines the resistance of the alloy electrode.

Appendix A. Relation between pressure and potential

The relation between the equilibrium potential (ΔE^0) of the metal hydride electrode and the equilibrium hydrogen pressure is given by the Gibbs free energy (ΔG):

$$\Delta G = RT \ln\left(\frac{p_{eq}}{p_0}\right) = -nF\Delta E^0 = \Delta H - T\Delta S$$

where R is the molar gas constant ($R = 8.31441$ Jmol^{-1}K^{-1}), T is the absolute temperature, p_{eq} is the hydrogen equilibrium pressure of the metal hydride, p_0 is the standard pressure (1.013×10^5 Pa which corresponds to a $\Delta E^0 = 0$), n is the number of electrons transfered in the reaction (2 electrons in the case of a metal hydride), F is the Faraday constant ($F = 96\,484.56$ A s mol^{-1}) and ΔE^0 is the equilibrium potential of the metal hydride electrode versus the standard hydrogen electrode ($\Delta E^0 = \Delta E_{MH} - \Delta E_{Hg/HgO}$). The use of a standard hydrogen electrode in an alkaline electrolyte is difficult, therefore a mercury/mercury oxide (Hg/HgO) electrode is usually applied as

reference electrode. The Hg/HgO reference electrode exhibits the same dependence on the pH like the hydrogen or the metalhydride electrode. Therefore the measured potentials of the metal hydride electrode referred to Hg/HgO are independent of pH. The standard potential of the Hg/HgO reference electrode at 20°C is $\Delta E_{Hg/HgO} = -926.9$ mV [12].

$$\ln\left(\frac{p_{eq}}{p_0}\right) = -\frac{2F}{RT}(\Delta E_{MH} - \Delta E_{Hg/HgO})$$

A potential change of 29.58 mV corresponds to change over a decade in pressure.

References

[1] H. Sawa, M. Ohta, H. Nakano, S. Wakao, Z. Phys. Chem. N. F. 164 (1989) 1527.

[2] C. Iwakura, M. Matsuoko, K. Asai, T. Kohno, J. Power Sources 38 (1992) 335.

[3] M. Matsuoka, K. Asai, Y. Fukumoto, C. Iwakura, J. Alloys and Compounds 192 (1993) 149.

[4] N. Kuriyama, T. Sakai, H. Miyamura, I. Uehara, H. Ishikawa, J. Alloys and Compounds 192 (1993) 161–163.

[5] N. Kuriyama, T. Sakai, H. Miyamura, I. Uehara, H. Ishikawa, T. Iwasaki, Journal of Alloys and Compounds 202 (1993) 183–197.

[6] A. Züttel, F. Meli, L. Schlapbach, J. of Alloys and Compounds 221 (1995) 207–211.

[7] Y. Fukumoto, M. Miyamoto, M. Matsuoka, C. Iwakura, Electrochimica Acta 7 (40) (1995) 845–848.

[8] C. Iwakura et al., J. Alloys and Compounds 259 (1997) 132–134.

[9] Y. Sakamoto, K. Kuruma, Y. Naritomi, Ber. Bunsenges. Phys. Chem. 96 (1992) 1813.

[10] A. Percheron-Guégan, J.-M. Welter, in: L. Schlapbach (Ed.), Hydrogen in Intermetallic Compounds I, Springer Series Topics in Applied Physics, Vol. 63, Springer–Verlag, 1988, p. 36, Chapter 2.

[11] M. Latroche, J. Rodríguez-Carvajal, A. Percheron-Guégan, F. Bourée-Vigneron, Journal of Alloys and Compounds 218 (1995) 64–72.

[12] J. Balej, Int. J. Hydrogen Energy 10 ((6)) (1985) 365–374, The temperature dependence of the standard potential of the Hg/HgO reference electrode is E [V] $= 1.18041 - (4.4666 \times 10^{-3} - 6.93606 \times 10^{-4} \ln(T))T - 1.0788 \times 10^{-6} \times T^2 + 4.512 \times 10^{-10} T^3 - 5.23 T^{-1}$.